Violation of hyperbolicity in a diffusive medium with local hyperbolic attractor

Pavel V. Kuptsov*
Department of Informatics, Saratov State Law Academy, Volskaya 1, Saratov 410056, Russia

Sergey P. Kuznetsov
Kotel'nikov Institute of Radio Engineering and Electronics, RAS, Saratov Branch, Zelenaya 38, Saratov 410019, Russia
(Received 28 December 2008; published 8 July 2009)

Departing from a system of two nonautonomous amplitude equations, demonstrating hyperbolic chaotic dynamics, we construct a one-dimensional medium as an ensemble of such local elements introducing spatial coupling via diffusion. When length of the medium is small, all spatial cells oscillate synchronously, reproducing the local hyperbolic dynamics. This regime is characterized by a single positive Lyapunov exponent. The hyperbolicity survives when the system gets larger in length so that the second Lyapunov exponent passes zero and the oscillations become inhomogeneous in space. However, at a point where the third Lyapunov exponent becomes positive, some bifurcation occur that results in violation of the hyperbolicity due to the emergence of one-dimensional intersections of contracting and expanding tangent subspaces along trajectories on the attractor. Further growth of the length results in the two-dimensional intersections of expanding and contracting subspaces that we classify as a stronger type of the violation. Beyond the point of the hyperbolicity loss, the system demonstrates an extensive spatiotemporal chaos typical for extended chaotic systems: when the length of the system increases the Kaplan-Yorke dimension, the number of positive Lyapunov exponents and the upper estimate for Kolmogorov-Sinai entropy grow linearly, while the Lyapunov spectrum tends to a limiting curve.

DOI: 10.1103/PhysRevE.80.016205 PACS number(s): 05.45.Jn, 47.27.Cn

I. INTRODUCTION

One of the central concepts in mathematical theory of dynamical systems relates to hyperbolic strange attractors. Tangent space of each point of such an attractor splits into expanding and contracting subspaces and this splitting is invariant. Dynamics on a hyperbolic attractor is structurally stable, i.e., is insensible to variations of parameters. It manifests strong stochastic properties and allows detailed theoretical analysis [1,2].

During the last 40 years, hyperbolic attractors were considered rather as idealized model of perfect chaos. Though some artificial systems with hyperbolic attractors were known, they were useless for practical applications because of complicated construction. Recently, a realistic system was suggested and implemented as an electronic device, dynamics of which in stroboscopic description is associated with the attractor of Smale-Williams type [3,4]. Attractor of this system is hyperbolic as proven numerically by verification of the cone criterion [5]. In paper [6], the amplitude equation for this system was studied and the hyperbolicity was also proven by the method of cones. (Some other models based on the same principle are considered in Refs. [7–10].)

Traditionally, studies of hyperbolic dynamics are mostly concentrated on low-dimensional systems. Many topics concerning spatiotemporal chaos, though attracted a lot of interest, remain open [11]. In this paper, we address a problem of survival of hyperbolicity of a spatiotemporal system when the length of the system grows. We consider a one-dimensional (1D) extended system composed of local elements possessing a hyperbolic attractor that is based on the amplitude equations from [6]. The spatial coupling is introduced via diffusion. In fact, a system we study is a set of two coupled nonautonomous Ginzburg-Landau equations of special form.

We are aware of two numerical methods for reliable verification of hyperbolicity. The first one is the method based on the cone criterion [5], which employs directly the rigorous theorem and, hence, looks preferable. Unfortunately, the method is appropriate only for low-dimensional systems, while its extension to systems of many degrees of freedom seems to be abundantly sophisticated. The second method is based on a recently suggested routine of computing of covariant Lyapunov vectors [12]. These vectors are associated with Lyapunov exponents and indicate directions of contracting and expanding manifolds at each point of an attractor. If these vectors are known, angles between each contracting and each expanding direction can be computed and the minimal one can be found. The attractor is interpreted as nonhyperbolic if distribution of these angles does not vanish at the origin. But in fact, this is only a sufficient condition because the converse is not true. In the present paper, we apply more subtle approach based on computation of so-called principal angles [13] that allows detecting a tangency of two arbitrary vectors from contracting and expanding subspaces.

The paper is organized as follows. In Sec. I, we introduce a system and briefly discuss its local dynamics. Also we describe a numerical method applied to find solutions to the system. Section II represents linear stability analysis. The critical length of the system is determined where a spatially homogeneous solution becomes unstable with respect to nonuniform perturbation. Section III is devoted to illustrations of spatiotemporal dynamics. The main part of the paper is Sec. IV, where we develop the Lyapunov analysis. We discuss

*Corresponding author; p.kuptsov@rambler.ru

distributions of minimal angles between contracting and expanding tangent subspaces on the attractor. Also, dependencies of Lyapunov exponents, Kaplan-Yorke dimension, and Kolmogorov-Sinai entropy on the length of the system are considered. In Sec. V, we summarize the obtained results and outline perspectives for further investigations.

II. MODEL AND NUMERICAL METHOD

Let us start with a physical model, demonstrating hyperbolic dynamics, suggested by Kuznetsov in Ref. [3]. The model consists of two coupled nonautonomous van der Pol oscillators that are parametrically influenced by an external periodic force. The oscillators become active turn by turn and pass the excitation each other in such way that the phase of oscillations is doubled after each period of the forcing. In Ref. [6], the amplitude equations for this system are derived that read

$$\dot{a} = A\cos(2\pi t/T)a - |a|^2 a - i\epsilon b,$$

$$\dot{b} = -A\cos(2\pi t/T)b - |b|^2 b - i\epsilon a^2. \quad (1)$$

In this paper, we study a spatially extended analog of these equations, supplying them with the second spatial derivatives.

So, we consider two coupled nonautonomous Ginzburg-Landau equations

$$\partial_t a = A\cos(2\pi t/T)a - |a|^2 a - i\epsilon b + \partial_x^2 a,$$

$$\partial_t b = -A\cos(2\pi t/T)b - |b|^2 b - i\epsilon a^2 + \partial_x^2 b. \quad (2)$$

Here, $a \equiv a(x,t)$ and $b \equiv b(x,t)$ are complex dynamical variables whose behavior is the subject of interest. Coefficients at linear terms undergo periodic variation with period T and amplitude A. The parameter modulation takes place in opposite phase for a and b. When the first subsystem is excited, the second one is relaxed and vice versa. The forcing is supposed to be slow, i.e., the half period $T/2$ is much longer then a transient time of the excitation. The second terms in the right-hand parts of the equations provide saturation of instabilities in the excited subsystems. Additionally, there are terms responsible for the coupling between a and b; the intensity of the coupling is controlled by ϵ. The coupling is asymmetric, being quadratic from a to b and linear in the inverse direction. Finally, the last terms in the right-hand parts introduce diffusion that is responsible for the spatial distribution of local oscillations. The diffusion coefficients of the subsystems are equal to 1. We study the system in a limited spatial domain $0 \le x \le L$. The boundary conditions are

$$(\partial_x a)_{|x=0,L} = (\partial_x b)_{|x=0,L} = 0. \quad (3)$$

Let us briefly discuss a local dynamics of the system. Consider Eqs. (1). (A more detailed study can be found in Ref. [6].) Due to the presence of the periodic forcing in Eq. (1), it is natural to introduce a stroboscopic map: we split the continuous time into steps of length T and consider a sequence of states of the system at the beginnings of these steps. Define phases within the interval $[0,2\pi)$: $\phi = \arg a$, $\psi = \arg b$. Suppose at some instant the first oscillator is excited and its amplitude $|a|$ is high. Then, the second one is suppressed and its amplitude $|b|$ is small. The coefficients in Eq. (1) are real except the coupling term. It means that the phases can vary only as a result of interaction between subsystems. But, when a is excited, $|b|$ is small and its action on a is negligible. Thus, the phase of a remains approximately constant during the excitation stage. On the contrary, the influence of the excited a on the suppressed b is strong. The coupling term is proportional to a^2. It means that after the half period $T/2$ at the threshold of its own excitation, the oscillator b inherits a doubled phase of a (also the phase gets the shift $-\pi/2$ because of the imaginary unit at the coupling term). Now the roles of subsystems are exchanged. Phase of b remains constant when this subsystem is excited and at the end, after the other $T/2$, the phase is returned back to a through a linear coupling term (also with the shift $-\pi/2$). As a result, the first oscillator a doubles its phase during the period T. This discussion allows to write down a map for a series of phases $\phi_n = \arg a(nT)$ that are measured over the time step T,

$$\phi_{n+1} = 2\phi_n - \pi \bmod 2\pi. \quad (4)$$

Up to a constant term (that can be eliminated by a shift of the origin of the phase), this map coincides with the well-known Bernoulli map [14,15]. It demonstrates chaotic dynamics and the chaos is homogeneous: a rate of exponential divergence of two close trajectories is identical at each point of the phase space, being equal to ln 2.

Getting back to the continuous system (1), we estimate its largest Lyapunov exponent as

$$\lambda_0 = \ln 2/T. \quad (5)$$

The described mechanism of phase doubling presumes a hyperbolic nature of the dynamics of Eq. (1). The numerical verification of the cone criterion, which has been preformed in Ref. [6], confirms this.

Before starting an analysis of the system (2), let us discuss a numerical method applied to find its solutions. Formally, our equations can be classified as parabolic partial differential equation (PDE). Typical recommendation of handbooks for such equations is the Crank-Nicolson method which is absolutely stable and provides the second order of local approximation both in space and in time. This method is semi-implicit, i.e., a solution at a new level t_{k+1} is expressed via previous solution at t_k as a set of algebraic equations, so that values from all spatial points on both levels are involved into this equation set. If PDE is linear, these equations are linear too. But application of this approach to nonlinear PDEs, such as ours, gives rise to a set of nonlinear algebraic equations that requires much more computational efforts. Usually, one simplifies the problem by neglecting terms, being nonlinear with respect to unknown variables. The resulting numerical scheme is semi-implicit for linear part of initial PDE and explicit for nonlinear part. Unfortunately, this simplified "quasi-Crank-Nicolson" method is not absolutely stable. Sometimes everything goes fine, but some-

times, usually when the system is far beyond the instability threshold, the solution diverges. In this paper, we do not neglect the nonlinearity and develop a true semi-implicit scheme. At each time step, we solve a set of nonlinear equations via the Newton-Raphson iterations. The seed for the iterations is found from the mentioned simplified method. The iterations converge very fast. Normally, it takes two or three repetitions to solve the nonlinear equations with the accuracy 10^{-5} or even better. The idea of the described method can be found in books on numerical analysis, e.g., [16,17]. Though the method is a bit complicated, this is compensated by its high accuracy and stability.

Below, different characteristic values are calculated as functions of the length of the system L. Varying L, we need to choose some strategy of simultaneous variation of parameters of a numerical mesh. One way is to keep constant number of points of the mesh N and compute space step as $\Delta x = L/(N-1)$. The other way is to fix the step Δx and find N for each L as $N=1+[L/\Delta x]$, where $\lceil\cdot\rceil$ means ceiling [to get a consistent numerical scheme, one also needs to adjust actual value of Δx for the equality $\Delta x(N-1)=L$ to fulfill]. In our simulations, we always keep constant N. This strategy seems to be preferable because the number of degrees of freedom of the numerical model remains constant; obviously, it is equal to $2N$ (traditionally defined as a half of a total order of the set of differential equations). So, we can be sure that phenomena, observed when L is varied, emerge due to a transformation of an inner structure of attractor and they cannot be attributed to just an extensive increase of degrees of freedom. The time step Δt can be either constant or attached to Δx. When Δt is sufficiently small, these two ways produce identical results. We shall hold the time step at $\Delta t \approx 0.01$. (Additionally, a small adjustment is also made to fit an integer number of steps into the observation interval). Though this is redundantly small value to obtain solutions to the system (2), but this is needed to estimate correctly its minor Lyapunov exponents.

III. LINEAR STABILITY ANALYSIS

Standard linear stability analysis of autonomous spatially extended active system requires a consideration of small perturbations to a homogeneous steady state. Existence of perturbation modes with positive growth rates indicates the instability of the homogeneous state. Our system does not have a steady state and its dynamics is chaotic in time. Oscillations can be either homogeneous or irregular in space. Our aim is to find the conditions for a transition from one regime to another, utilizing ideas of the standard analysis.

Suppose that the system is infinite in space and its initial state is uniform. Prepared in this way, the system obviously demonstrates homogeneous oscillations; at any spatial point, the dynamics can be described by the ordinary differential equations (ODE) system (1). Let us consider an inhomogeneous perturbation to these oscillations. We need to seek a solution composed as a sum of a homogeneous part, say, $a_0(t)$ and $b_0(t)$, and a sinusoidal mode of perturbation with real wave number k and real growth rate $\sigma(k)$. The system is chaotic; thus, instead of usual assumption of time periodicity of small perturbation, we introduce small amplitudes $\tilde{a}(t)$ and $\tilde{b}(t)$ and require them neither grow nor decay, in average. It means that there exist two constants, $0<K<M<\infty$, such that $K<|\tilde{a}(t)|<M$ and $K<|\tilde{b}(t)|<M$ for $t>0$. So, we set

$$a(x,t) = a_0(t) + \tilde{a}(t)e^{\sigma(k)t - \mathrm{i}kx},$$

$$b(x,t) = b_0(t) + \tilde{b}(t)e^{\sigma(k)t - \mathrm{i}kx}. \tag{6}$$

After substitution of Eq. (6) to Eq. (2), we exclude nonlinear terms in $\tilde{a}$ and $\tilde{b}$, supposed to be small, and obtain a set of linear ODE for complex amplitudes of perturbation

$$\dot{\tilde{a}} = [A\cos(2\pi t/T) - \lambda_0]\tilde{a} - 2|a_0|^2\tilde{a} - a_0^2\tilde{a}^* - \mathrm{i}\epsilon\tilde{b},$$

$$\dot{\tilde{b}} = [-A\cos(2\pi t/T) - \lambda_0]\tilde{b} - 2|b_0|^2\tilde{b} - b_0^2\tilde{b}^* - 2\mathrm{i}\epsilon a_0\tilde{a}, \tag{7}$$

where $\lambda_0 = k^2 + \sigma(k)$ and asterisks denote the complex conjugation. A value of λ_0 controls growth or decay of a solution. Because $\tilde{a}(t)$ and $\tilde{b}(t)$ should be bounded at any k, λ_0 does not depend on k. One can easily check that Eq. (7) also describes small perturbation to an orbit of Eq. (1). It means that the conditions on $\tilde{a}(t)$ and $\tilde{b}(t)$ are fulfilled when λ_0 is equal to the largest Lyapunov exponent of Eq. (1). Thus, we can write

$$\sigma(k) = \lambda_0 - k^2. \tag{8}$$

Relation (8) can be verified by direct numerical computations of $\sigma(k)$. For this purpose, we substitute $\lambda_0 \to \sigma(k) + k^2$ to Eq. (7) and set there $\sigma(k)=0$. It means that now the amplitudes $\tilde{a}$ and $\tilde{b}$ are allowed to grow or decay, so that the rate will be equal to $\sigma(k)$. Given k, we find $\sigma(k)$ employing the algorithm of computing of the largest Lyapunov exponent [18]. System (7) is initialized with a unit vector and then solved together with Eq. (1) on one period T. After that, a norm of the vector solution of Eq. (7) is found and stored and the vector itself is normalized. When this procedure is repeated for a sufficiently long time, averaged logarithms of the collected norms determine the sought $\sigma(k)$. The results are shown in Fig. 1. Solid lines represent theoretical $\sigma(k)$ in Eq. (8). The upper one corresponds to a hyperbolic chaos in Eq. (1) and λ_0 is found according to Eq. (5). The lower curve also corresponds to chaotic oscillations of Eq. (1) that are, however, nonhyperbolic. In this case, we substitute a computed value of $\sigma(0)$ to Eq. (8) instead of λ_0. Numerical data fit well the theoretical curves. As follows from Eqs. (5) and (8), $\sigma(k)$ does not depend on A in the regime of hyperbolic chaos. Numerical verification confirms this.

Linear modes described by Eq. (7) are influenced parametrically by a chaotic force. It means that all modes with positive $\sigma(k)$ can grow simultaneously giving rise spatiotemporal chaos. The spectrum of lineally unstable modes with $\sigma(k)>0$ can be found in Eq. (8). These modes lay within the interval of wave numbers $0 \le k < k_{\mathrm{lin}}$, where

$$k_{\mathrm{lin}} = \sqrt{\lambda_0}. \tag{9}$$

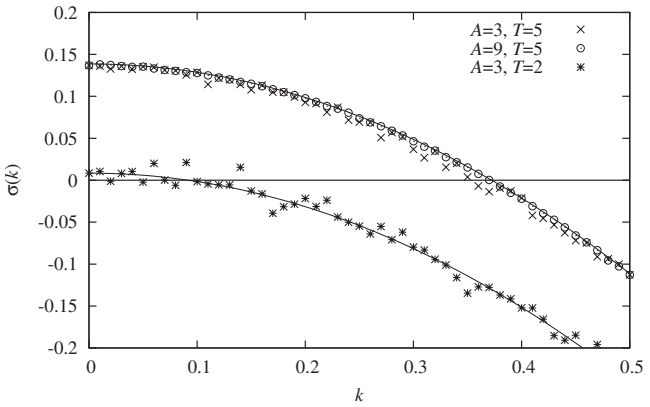

FIG. 1. Growth rate $\sigma(k)$ of nonuniform perturbation to a homogeneous solution of the system (2). Solid curves are the graphs of Eq. (8): the upper one is $(\ln 2)/5-k^2$ and the lower one is $\sigma(0)-k^2$, where $\sigma(0)=0.008\,42$. Crosses, circles, and stars represent numerical data, computed at parameters that are shown in the legend.

If the system (2) is bounded by the length L, the spectrum of modes allowed by the boundary conditions (3) is

$$k_n = n\pi/L, \quad n = 1,2,3,\ldots. \tag{10}$$

When L is small, so that $k_1 > k_{\text{lin}}$, there are no unstable eigenmodes and the system demonstrates homogeneous oscillations. Spatial structure emerges above the critical point which can be found from the condition $k_1 = k_{\text{lin}}$: $L_c = \pi/\sqrt{\lambda_0}$. Below, we put an attention to the case when the local dynamics is hyperbolic. The Lyapunov exponent λ_0 in this case is given by Eq. (5) and the critical length reads

$$L_c = \pi\sqrt{T/\ln 2}. \tag{11}$$

IV. SPATIOTEMPORAL DYNAMICS

Let us consider some illustrations of spatiotemporal dynamics of the system (2). Figure 2 represents homogeneous oscillations. In this and subsequent figures, the space coordinate is horizontal, time is directed vertically, and gray levels

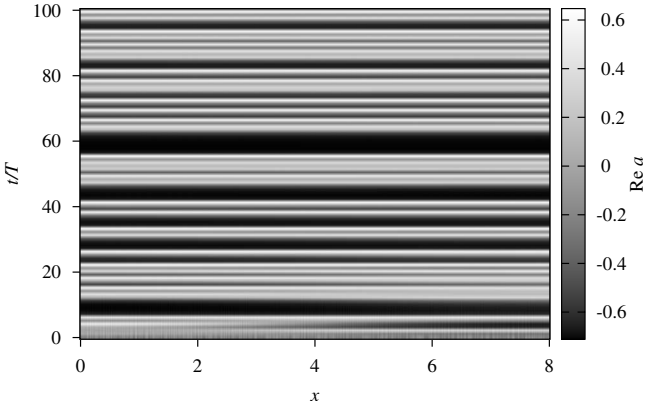

FIG. 2. Spatiotemporal dynamics of Eq. (2) at $L=8$. Gray levels indicate values of Re a. $A=3$, $T=5$, and $\epsilon=0.05$.

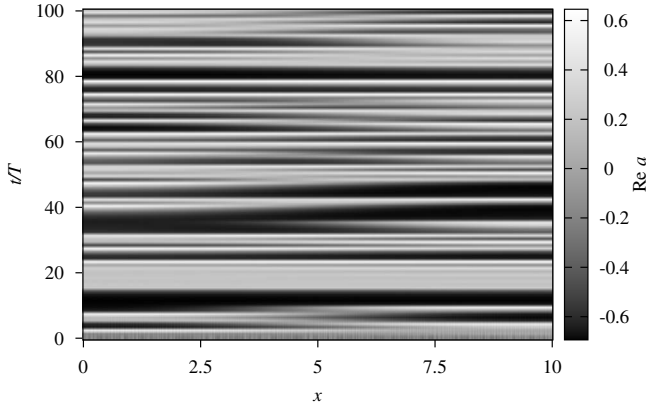

FIG. 3. Same as Fig. 3, but at $L=10$.

indicate values of Re a as shown by gradient bars at the right edges of the diagrams. Layers Re $a(x)$ are plotted at successive steps $t_n = nT$. Critical length, according to Eq. (11), is $L_c \approx 8.44$. The length of the system in Fig. 2 is less then the critical value, $L=8$. Hence, after a short transient time, it settles in a regime of homogeneous oscillations.

In Fig. 3 the length $L=10$ is larger than L_c. The first eigenmode $\cos(k_1 x)$ falls into the instability domain and grows, destroying the homogeneity. The first mode contains one half of the period of cosine, so if a maximum is at the left edge of the system, a minimum appears at the right edge and vice versa. Careful inspection of Fig. 3 confirms this conclusion. If a horizontal stripe, representing Re $a(x)$ at a certain time step, is white at the left edge, it becomes dark at the right edge.

The result of further increase of the length up to $L=500$ is shown in Fig. 4. As here a lot of eigenmodes satisfy the condition $k_n < k_{\text{lin}}$, they are exited and produce a rich and complicated structure. It is interesting to note that it reminds a structure generated by cellular automata of Wolfram's class 3 [19].

V. LYAPUNOV ANALYSIS

Lyapunov exponents are average rates of expansion or contraction in the tangent space on an attractor. They characterize sensitivity of motion to small perturbations; the at-

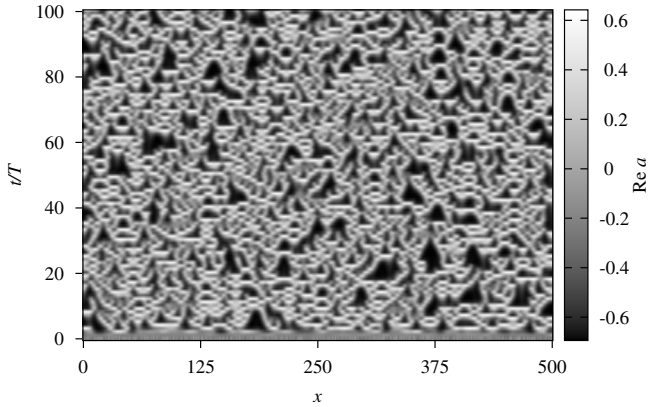

FIG. 4. $L=500$.

tractor with a positive exponent is chaotic. Also, it is important to know a mutual orientation of expanding and contracting directions in the tangent space at each point of the attractor. This information can be provided by covariant Lyapunov vectors [12]. If there is a well-defined split of the tangent space into contracting and expanding subspaces, the dynamics is hyperbolic. On the contrary, the dynamics is nonhyperbolic when couples of collinear vectors from contracting and expanding subspaces can be encountered with a nonzero probability.

In this section, we compute covariant Lyapunov vectors and perform a verification of hyperbolicity of the attractor of Eq. (2). Also, we analyze Lyapunov exponents for the system (2) as well as related to them Kaplan-Yorke dimension and Kolmogorov-Sinai entropy.

A. Verification of hyperbolicity at different lengths of the system

To verify the hyperbolicity, one needs to analyze expanding and contracting directions in the tangent space on an attractor. These directions can be found in a form of covariant Lyapunov vectors [12]. The method of computation of these vectors is briefly described in the Appendix.

When the covariant Lyapunov vectors are computed at some point of the attractor, the simplest way to verify the hyperbolicity is to compute angles between each couple of expanding and contracting vectors and find the smallest one. Collecting the smallest angles for sufficiently many points, one obtains a sufficient condition for nonhyperbolicity: the attractor is nonhyperbolic if zero angle can be encountered with a nonzero probability. But the converse is not true. The covariant Lyapunov vectors may not be collinear themselves, but the loss of hyperbolicity still can take place due to a tangency of some other couple of vectors from contracting and expanding subspaces. To take this situation into account, a more subtle approach should be used.

Let us suppose that at some point of the attractor, we have n_s covariant Lyapunov vectors spanning the contracting tangent subspace $\mathcal{S}$ and n_u vectors that span the expanding subspace $\mathcal{U}$. It is natural to assume that $n_s > n_u$. Consider unit vectors $s \in \mathcal{S}$ and $u \in \mathcal{U}$ and find among them a couple s_1 and u_1 that produces the largest inner product. Arc cosine of $s_1^T u_1$ is the smallest angle between subspaces, which is denoted as θ_1. Then we seek for unit vectors s_2 and u_2 that again produce the largest inner product but with additional requirement to be orthogonal to s_1 and u_1, respectively. Arc cosine of their inner product is denoted as θ_2. Proceeding with this procedure, we obtain n_u angles

$$0 \le \theta_1 \le \cdots \le \theta_{n_u} \le \pi/2, \tag{12}$$

which are called the principal angles. Corresponding vectors s_i and u_i are called the principal vectors. The formal definition of the principal angles and vectors is the following [13]:

$$\cos\ \theta_k = \max_{s \in \mathcal{S}} \max_{u \in \mathcal{U}} s^T u = s_k^T u_k, \tag{13}$$

where

$$s^T s = u^T u = 1,$$

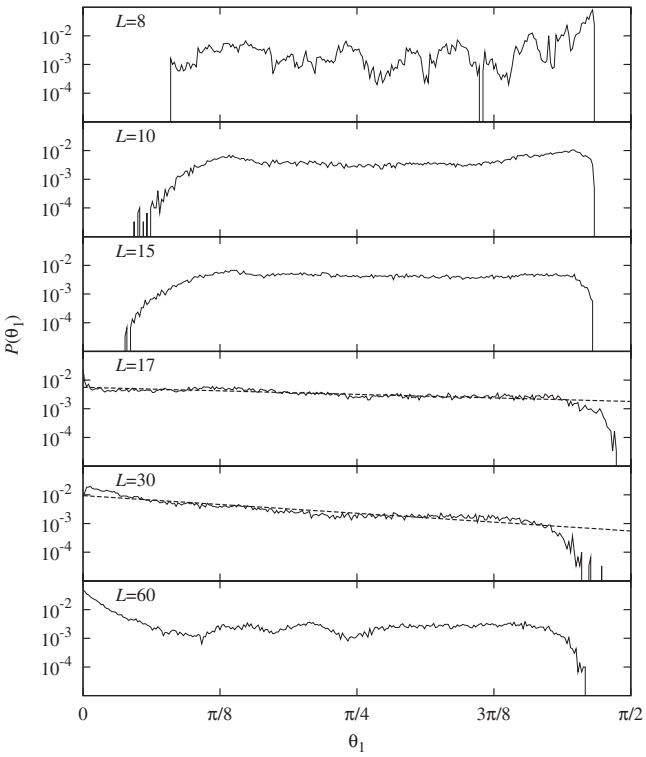

FIG. 5. Distributions of minimal angles θ_1 between contracting and expanding tangent subspaces of the attractor of Eq. (2). $A=3$, $T=5$, and $\epsilon=0.05$. The logarithmic scale is used along the ordinate axis. Dashed lines in the panels $L=17$ and $L=30$ are obtained via least-squares fit. There is one positive Lyapunov exponent at $L=8$, two at $L=10$ and $L=15$, three at $L=17$, five at $L=30$, and 11 at $L=60$. Observe the violation of hyperbolicity at $L>15$, i.e., when the third Lyapunov exponent becomes positive.

$$s^T s_i = 0, \quad u^T u_i = 0, \quad i = 1, \ldots, k-1. \tag{14}$$

The algorithm of computation of the principal angles is discussed in the Appendix.

The vanishing of the principal angles indicates the tangency between contracting and expanding subspaces and the violation of hyperbolicity. A necessary and sufficient condition for the loss of hyperbolicity is the appearance on the attractor of such a distribution of θ_1 that has a nonzero value at the origin. If a system has many degrees of freedom, several smallest principal angles can vanish simultaneously, which means that several couples of contracting and expanding vectors merge. A number of such angles defines the dimension of the tangency. A necessary and sufficient condition for the n-dimensional tangencies is a nonzero probability of vanish of the sum of first n principal angles.

Figure 5 represents distributions of θ_1 for the system (2) at different lengths L. The equations have been solved at $\Delta t \approx 0.01$ and $\Delta x = L/(N-1)$, where N is the number of points of a numerical mesh. $N=51$ for all L, except $L=60$ where $N=101$. The distributions have been computed with the resolution 300 points. For each distribution, ten trajectories of the length $600T$ have been processed with the interval $T/30$ between renormalizations and orthogonalizations (see the Appendix for details). In the course of the backward it-

erations, a time interval $500T$ is omitted as transient and then the angles are computed on the interval $100T$. Thus, totally, 3000 angles for each trajectory have been stored. The distributions have been normalized, $\int_0^{\pi/2} P(\theta_1)=1$.

The upper curve $L=8$ in Fig. 5 corresponds to a spatially homogeneous case. The angles are very well localized. Thus, the hyperbolic dynamics is observed that corresponds to the hyperbolic dynamics of the ODE system (1). The second curve $L=10$ represents the case of a weak inhomogeneity when the system is not far above the critical point L_c. Observe that the distribution becomes much smoother compared to the homogeneous case. It means that different configurations of contracting and expanding subspaces are encountered with almost equal probabilities. The distribution is still separated well from the origin, i.e., the attractor remains hyperbolic. This is also the case for the next distribution at $L=15$. This distribution is even flatter than the previous one and also it is separated well from the origin. Notice that there are two positive Lyapunov exponents both at $L=10$ and at $L=15$. The picture becomes dramatically different at $L=17$ when the third Lyapunov exponent becomes positive. The distribution occupies almost the whole range of angles and has nonzero value at origin. The former indicates that the attractor becomes nonhyperbolic. Moreover, notice that in the logarithmic scale, the curve decays linearly from the origin. It means that the most part of the distribution is described by an exponential function. Similar behavior is observed at $L=30$: the most part of the curve obeys the exponential law. The exponents, which are equal to the slopes of the dashed approximating lines, are -0.72 at $L=17$ and -1.81 at $L=30$, i.e., their absolute values grow with L. When L gets larger, as in the panel for $L=60$, the distribution undergoes a transformation. It acquires an extended sloping segment near the origin, while the other part of the distribution becomes more or less flat, on average. The attractor remains nonhyperbolic and, moreover, the probability to encounter the tangency of contracting and expanding subspaces becomes larger.

We can assume that the reorganization of the structure of distribution, which occurs between $L=30$ and $L=60$, is associated with emergence of the two-dimensional tangencies of contracting and expanding subspaces. Figure 6 demonstrates distributions of two first principal angles $(\theta_1+\theta_2)/2$. The curve at $L=17$ is separated well from the origin, so that no two-dimensional tangencies take place. At $L=30$, the curve approaches zero much closer. Finally, the curve at $L=60$ touches the ordinate axis, confirming the presence of the two-dimensional tangencies.

Figure 7 reproduces the observed scenario at some other set of parameters. In panel (a), we can see that the attractor is hyperbolic with two positive Lyapunov exponents, curve $L=10$, while emergence of the third one results in the violation of the hyperbolicity, curve $L=11$. Similar to the case presented in Fig. 5, the distribution right above the violation point is basically exponential, curve $L=11$, while the further growth of L results in the transformation of the distribution, curve $L=60$. Figure 7(b) indicates the emergence of the two-dimensional tangencies in this case: the distributions of $(\theta_1+\theta_2)/2$ approach the origin as L grows and touch it at $L=60$.

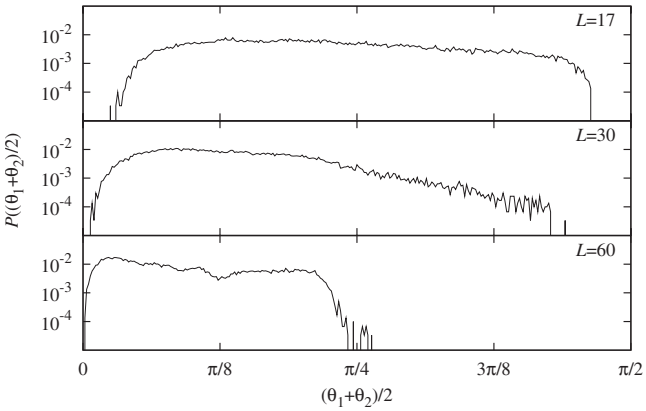

FIG. 6. Distributions of two principal angles $(\theta_1+\theta_2)/2$. Observe how curves approach the origin and touch it at $L=60$, which indicates the two-dimensional tangencies between contracting and expanding subspaces. The parameters are as in Fig. 5.

So we observe that the growth of L first results in the violation of hyperbolicity due to one-dimensional tangencies of contracting and expanding subspaces and then gives rise to two-dimensional tangencies between these subspaces. It is natural to suggest that the tangencies of higher dimensions also arise at appropriate lengths of the system. The violation

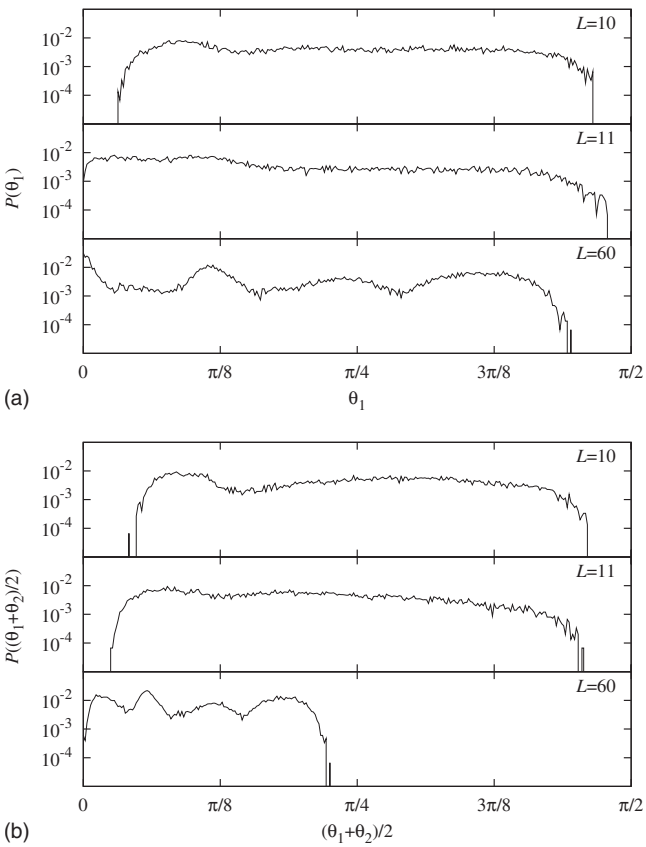

FIG. 7. Distributions of θ_1 and $(\theta_1+\theta_2)/2$, panels (a) and (b), respectively, at $A=8$, $T=2$, and $\epsilon=0.05$. There are two positive Lyapunov exponents at $L=10$, three at $L=11$, and 16 at $L=60$. Observe the violation of hyperbolicity at $L=11$ in the (a) and the emergence of two-dimensional tangencies at $L=60$ in (b).

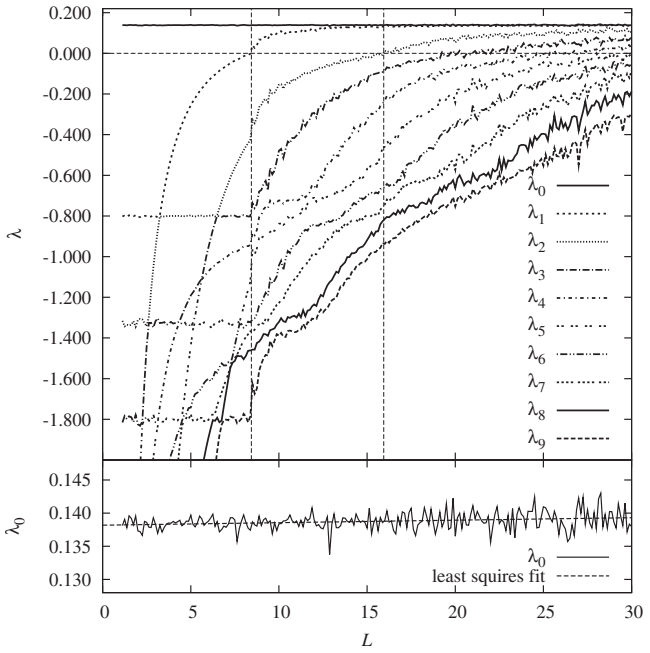

FIG. 8. Ten largest Lyapunov exponents of the system (2) against L. $A=3$, $T=5$, and $\epsilon=0.05$. Vertical dashed lines mark $L_c \approx 8.44$ and $L_2 \approx 15.9$ (the point where $\lambda_2=0$). Lower panel represents λ_0 in a large scale. Dashed approximating line, $4\times10^{-5}L+0.138$, is obtained via least-squares fit.

of hyperbolicity is accompanied by the emergence of the third positive Lyapunov exponent. Let us denote the point where the third Lyapunov exponent passes zero as L_2. We suspect that the loss of hyperbolicity takes place exactly at $L=L_2$ and below, additional evidences of this assertion are presented.

B. Lyapunov exponents against the length of the system

Figure 8 represents the Lyapunov exponents λ_i as functions of L. The plots are obtained at $N=51$ points of the spatial mesh, $\Delta x=L/(N-1)$ and $\Delta t \approx 0.01$. The interval between renormalizations and orthogonalizations is $T/30$ (see the Appendix for details). Notice that the zero exponent is absent. This is natural for the nonautonomous system we deal with.

The largest exponent λ_0 remains almost constant as L varies (see the lower panel in Fig. 8). The approximating line, obtained via least-squares fit, does not have a noticeable slope (the slope is of the order 10^{-5}) and is plotted at constant value 0.138. This is equal with a remarkable accuracy to the theoretically predicted largest Lyapunov exponent (5) of the corresponding ODE system (1). When L is small, the system has the single positive exponent that corresponds to spatially homogeneous chaotic oscillations. As L grows, the second exponent λ_1 becomes positive at $L=L_c$. This indicates the transition to a spatially inhomogeneous solution. Further increase of L results in a cascade of passing through zero of the exponents.

Figure 9(a) shows lengths L_n where corresponding Lyapunov exponents λ_n vanish. Two lines correspond to two

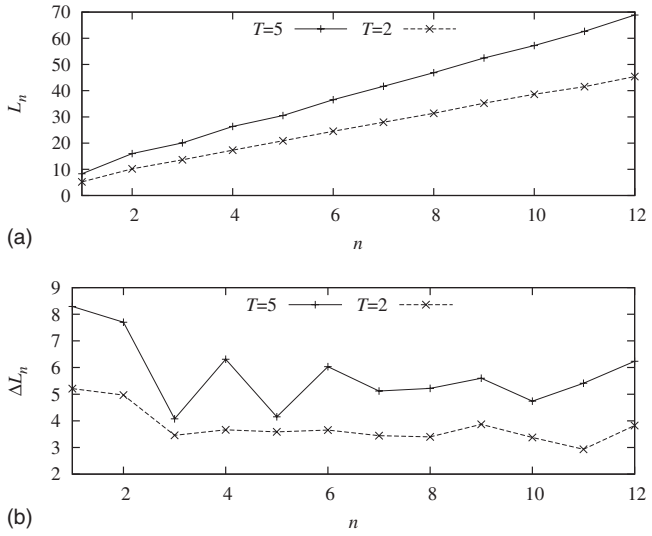

FIG. 9. (a) Values of length L_n where corresponding Lyapunov exponents λ_n pass zero and (b) intervals between these points $\Delta L_n=L_n-L_{n-1}(\Delta L_1 \equiv L_c)$. Solid lines on both panels correspond to the parameters $A=3$, $T=5$, and $\epsilon=0.05$, and dashed lines represent parameters $A=8$, $T=2$, and $\epsilon=0.05$.

sets of parameters of the system. One can see that L_n depends linearly on n. It means that the number of positive exponents also linearly, on average, grows with L. In Fig. 9(b), the intervals $\Delta L_n=L_n-L_{n-1}$ are plotted ($\Delta L_1 \equiv L_c$). Notice that $\Delta L_2 \approx \Delta L_1$ and these two values are larger then the others ΔL_n. We attribute this to the transition to a nonhyperbolic attractor that takes place at L_2.

C. Kaplan-Yorke dimension and Kolmogorov-Sinai entropy

Figure 10 illustrates the Kaplan-Yorke or Lyapunov dimension D_{KY} [14,15] and the sum of positive Lyapunov exponents h_μ, which is an upper estimate for the Kolmogorov-Sinai or metric entropy [14,15]. Two panels are obtained for different sets of parameters. Vertical dashed lines mark the point L_c of transition to the spatially inhomogeneous attractor and the point L_2, where the third Lyapunov exponent passes zero so that the attractor becomes nonhyperbolic.

Let us consider h_μ in more details. It is known that for a hyperbolic attractor, h_μ is equal to its Kolmogorov-Sinai entropy, while for a generic chaotic attractor this is an upper estimate for the entropy [15]. Because our system is hyperbolic at $L<L_2$, we can use h_μ to construct a function which approximates the entropy at least on this interval. Below L_c, we have $h_\mu=\lambda_0$, while above this point, h_μ demonstrates a power-law behavior. Thus, employing the least-squares fit, we obtain a function, approximating h_μ as

$$\chi_\mu(L)=\begin{cases}\lambda_0 & L \le L_c \\ \alpha(L-L_c)^\gamma+\lambda_0 & L > L_c,\end{cases} \tag{15}$$

where $\alpha=0.083$ and $\gamma=0.25$ for Fig. 10(a) and $\alpha=0.229$ and $\gamma=0.26$ for Fig. 10(b). The indices γ computed for different parameter sets are, perhaps, identical (small difference can be attributed to errors of computations).

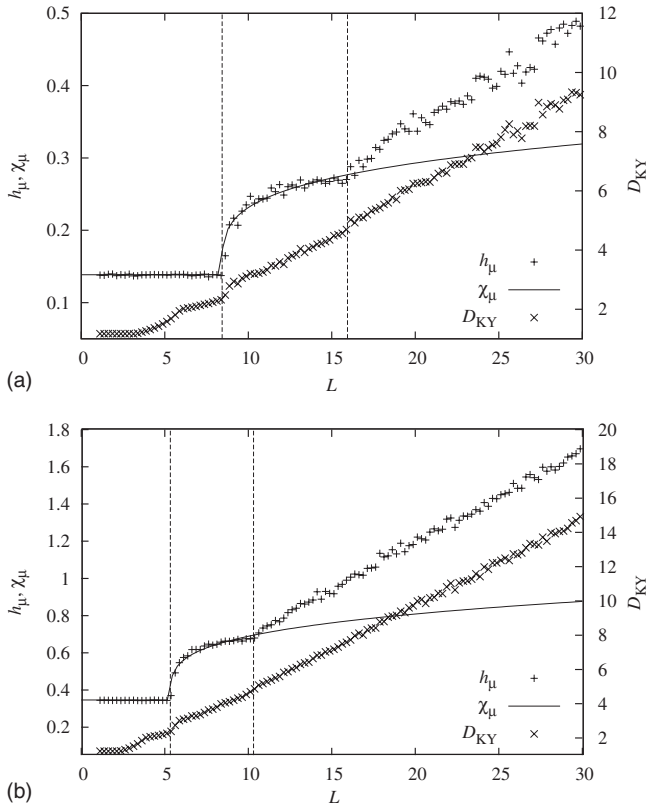

FIG. 10. Kaplan-Yorke dimension D_{KY}, upper estimate h_μ for the Kolmogorov-Sinai entropy, and its power law approximation χ_μ (15) against L. (a) $A=3$, $T=5$, and $\epsilon=0.05$. (b) $A=8$, $T=2$, and $\epsilon=0.05$. Vertical dashed lines mark L_c and L_2.

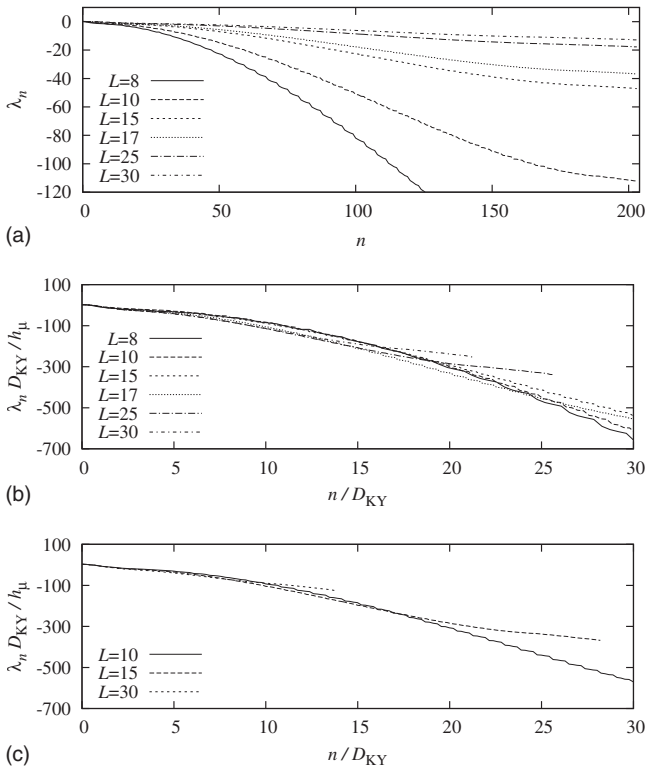

FIG. 11. (a) Spectra of Lyapunov exponents and (b) scaled spectra at $A=3$, $T=5$, and $\epsilon=0.05$. (c) Scaled spectra at $A=8$, $T=2$, and $\epsilon=0.05$.

The power-law approximation (15) agrees very well with the numerical curve h_μ at $L<L_2$ and at $L=L_2$, a bifurcation occurs that is associated with the loss of hyperbolicity. There are two possibilities above this point. The first one is that the Eq. (15) still gives correct value of the entropy, while h_μ serves as an upper estimate. The other possibility is that h_μ correctly represents the entropy, while the approximation (15)) becomes inappropriate. Anyway, both of these variants fit well with our conclusion that the system loses the hyperbolicity at $L=L_2$.

Above L_2, the entropy h_μ grows linearly with the length as well as the dimension. A number of positive Lyapunov exponents also demonstrates a linear growth as follows from the linear growth of L_n in Fig. 9(a). This is a typical phenomenon for extensive fully developed chaos in extended systems. In particular, the linear growths of $D_{KY}(L)$ and $h_\mu(L)$ were reported for coupled map lattices [20], for Kuramoto-Sivashinsky (KS) equation [21], and for complex Ginzburg-Landau (CGL) equation [22]. Also, the linear growth of D_{KY} was demonstrated for a chaotic attractor of coupled Ginzburg-Landau equations [23]. It can be explained by exponential decay of spatial correlations. Two points with space separation larger than the correlation length move independently, so that the system can be roughly represented by a direct product of independent subsystems [20]. Thus, the additivity is observed: the growth of L merely results in the proportional increase of the characteristic values.

D. Spectra of Lyapunov exponents

Figure 11(a) demonstrates spectra of Lyapunov exponents at different L. The first curve $L=8$ corresponds to a spatially homogeneous case when oscillations in all spatial points are synchronized and can be described by Eq. (1). There is one positive Lyapunov exponent. As one can see from the figure, the minor negative exponents have very large absolute values. It means that only a few spatial modes are actually involved in the dynamics, while the most of modes are highly damped. When L grows, more Lyapunov exponents become positive and the remaining negative exponents approach the axis of abscissas so that their absolute values become smaller. In the other words, more spatial modes participate in the dynamics. The separation of modes involved and not involved in the observable dynamics is studied in Ref. [24]. For a dissipative chaotic system, it is shown to exists a splitting of the tangent space into physical modes, responsible for the observable dynamics, and hyperbolically isolated from them highly damped nonphysical modes that do not bring an essential information about the dynamics.

For a fully developed spatiotemporal chaos, a Lyapunov spectrum scaled as $(D_{KY}/h_\mu)\lambda(n/D_{KY})$ is known to tend to a limiting curve at $L\to\infty$. In particular, this was reported for coupled map lattice [20], for KS equation [21], and for CGL equation [22]. Figures 11(b) and 11(c) represent the verification of this property for the system (2) at two sets of parameters. One can see high correspondence of curves obtained at different L.

VI. SUMMARY AND CONCLUSION

We considered an extended system whose local dynamics is hyperbolic and spatial coupling is introduced via diffusion. A numerical verification of hyperbolicity of the attractor of this system was performed. The test was based on the computation of distributions of principal angles between contracting and expanding tangent subspaces of the attractor. The analysis revealed that the hyperbolicity is inherent only to a low-dimensional chaos observed at sufficiently small lengths of the system.

The dynamics is obviously hyperbolic when oscillations are homogeneous in space because each spatial cell merely reproduces the oscillations of a partial ODE system that is known to be hyperbolic. This regime is characterized by a single positive Lyapunov exponent. The hyperbolicity survives when the length gets larger, so that the first spatial mode allowed by boundary conditions becomes linearly unstable and the oscillations become inhomogeneous. This transition is accompanied by the emergence of the second positive Lyapunov exponent. Further growth of the length results in the emergence of the third positive Lyapunov exponent. In this point, the violation of hyperbolicity takes place.

Beyond the point of the hyperbolicity loss, the system demonstrates an extensive spatiotemporal chaos that is characterized by a fast decay of a spatial correlation. We verified several standard criteria and observed behavior that is typical for many other extended chaotic systems. Namely, the number of positive Lyapunov exponents, the sum of positive exponents (this value is an upper estimate for Kolmogorov-Sinai entropy), and the Kaplan-Yorke dimension grow linearly against the length of the system. Spectrum of the Lyapunov exponents, being properly rescaled, tends to a limiting curve as the length grows.

So, if the length of the system grows and the third Lyapunov exponent becomes positive, we register the violation of hyperbolicity due to the emergence of one-dimensional intersections of contracting and expanding tangent subspaces of the attractor. If the length continues to increase, along with one-dimensional intersections, we observe two-dimensional ones. This is a stronger type of the hyperbolicity violation because there is higher probability for the perturbation to be transferred between contracting and expanding subspaces. We expect that the intersections of higher dimensions also take place as the length diverges. It is interesting to study the violation of hyperbolicity in the thermodynamic limit. If the number of modes involved in the dynamics is infinite, the maximal dimension of the intersections may be infinite too or it can have a finite value. The first case can be termed as a strong violation because the capacity of set of the merging vectors from contracting and expanding subspaces is comparable with the capacity of the whole set of degrees of freedom. Hence, the probability for the perturbation to be transferred between contracting and expanding subspaces is nonzero. The second case can be termed as a weak violation. Though the intersections take place, the number of merging directions per degree of freedom is zero. Thus, the probability of the perturbation transfer vanishes.

ACKNOWLEDGMENTS

P.V.K. acknowledges support from RFBR-DFG under Grant No. 08-02-91963, and S.P.K. acknowledges support from RFBR under Grant No. 09-02-00426.

APPENDIX: COMPUTATION OF LYAPUNOV EXPONENTS, COVARIANT LYAPUNOV VECTORS, AND ANGLES BETWEEN SUBSPACES

To compute Lyapunov exponents, we apply an algorithm based on the QR decomposition. See Refs. [25–27] for the details of the algorithm and Ref. [13] for an idea of the QR decomposition.

First of all, equations for small perturbations $\tilde{a}(x,t)$ and $\tilde{b}(x,t)$ to trajectories $a(x,t)$ and $b(x,t)$ of Eq. (2) are required

$$\partial_t \tilde{a} = A\cos(2\pi t/T)\tilde{a} - 2|a|^2\tilde{a} - a^2\tilde{a}^* - \mathrm{i}\epsilon\tilde{b} + \partial_x^2\tilde{a},$$

$$\partial_t \tilde{b} = -A\cos(2\pi t/T)\tilde{b} - 2|b|^2\tilde{b} - b^2\tilde{b}^* - 2\mathrm{i}\epsilon a\tilde{a} + \partial_x^2\tilde{b}, \tag{A1}$$

where asterisks denote the complex conjugation. To compute M_λ Lyapunov exponents, we need M_λ exemplars of the linear equation sets (A1), which are initialized by an orthogonal set of random unit vectors of the length $4N$, where N is the number of points of a numerical mesh. Basic system (2) is also initialized and advanced along a trajectory for a sufficiently long time to arrive at the attractor. Then, the basic system is solved simultaneously with M_λ linear equation sets during some time interval. The more Lyapunov exponents are required, the shorter interval should be taken because minor negative Lyapunov exponents can have very large absolute values so that the corresponding solutions of linear subsystems decay very fast. M_λ resulting vectors are then considered as columns of a matrix that is decomposed into an orthogonal matrix Q and an upper triangular matrix R. (An algorithm based on the Householder rotation is used [13].) Logarithms of M_λ diagonal elements of the R are collected, while M_λ columns of the Q are used to reinitialize linear systems. Then this procedure is repeated. Averaged logarithms of diagonal elements of R converge to Lyapunov exponents.

To compute covariant Lyapunov vectors according to the method recently reported in Ref. [12], we must do the similar things. After initialization of the equations, we make several steps n_0 accompanied by the QR procedure, but without storing elements of R, to obtain a good matrix Q_{n_0}. "A good" means that each linear subspace $\mathcal{S}^j_{n_0}$, $j=1,2,\ldots 4N$, spanned by first j vector columns of Q_{n_0}, contains jth expanding (or contracting) direction of the tangent space at n_0. Starting from n_0, we make some more steps and arrive at n_1. Here we have a matrix Q_{n_1} with columns that determine subspaces $\mathcal{S}^j_{n_1}$. Our aim now is to define arbitrary unit vectors belonging to these subspaces, $u^j_{n_1} \in \mathcal{S}^j_{n_1}$, $j=1,2\ldots 4N$. In fact, we just need to generate a random upper triangular matrix C_{n_1}, whose size coincides with R and columns are normalized by 1. jth column of C_{n_1} contains coordinates of $u^j_{n_1}$ with respect to the basis Q_{n_1}. In other words,

$$U_n = Q_n C_n, \tag{A2}$$

where $U_n = \{u_n^1, u_n^2, \ldots, u_n^{4N}\}$. Starting from C_{n_1}, we perform backward iterations $C_{n-1} = R_n^{-1} C_n$ accompanied by renormalization of columns of C_n. Collecting and averaging the negative logarithms of the norms, we obtain Lyapunov exponents. Under these iterations the, vectors u_n^j, represented by columns of the C_n, are aligned with the most expanding directions of subspaces $\mathcal{S}_n^j$. These directions are associated with corresponding Lyapunov exponents. Because we go back in time, the highest Lyapunov exponents do not dominate this alignment. If the number of steps from n_1 to n_0 is sufficiently large, getting back at n_0, we obtain the matrix C_{n_0} with coordinates of covariant Lyapunov vectors U_{n_0}, pointing expanding and contracting directions of the tangent space at n_0. Explicit form of U_{n_0} can be found from Eq. (A2). Computed in parallel, the Lyapunov exponents allow to distinguish expanding and contracting directions.

In practice, computing the covariant Lyapunov vectors for a system of many degrees of freedom, we must deal with very large arrays of data. For the backward procedure to be performed, $m = n_1 - n_0$ matrices R should be stored. The time interval between successive QR decompositions should be sufficiently small to treat minor Lyapunov exponents and corresponding vectors accurately, while the duration of the backward procedure must be long because the vectors are found to converge sufficiently slow. As a result, an array of matrices R runs up to several gigabytes. We recall that on 32-bit platforms, the physical limit of an addressable memory is 4 Gb, while the memory actually available for programs is even less. It means that we cannot store such array in memory and need to write it to a file. (Otherwise, one can employ a 64-bit platform with appropriate amount of memory, of course.) Moreover, the file must be written in a binary format. The usual text format is not a saving so that an extremely large file can be obtained.

According to Eq. (A2), we need Q_{n_0} to restore covariant Lyapunov vectors in the original phase space. It means that an array of m matrices Q must also be stored. Hopefully, this is not needed. The transformation (A2) preserves angles because matrices Q_n are orthogonal. Thus, we do not need the U_n to analyze the structure of the tangent space. Identical information about this space can be extracted directly from the column space of C_n.

To compute the C_n, we apply a two-pass procedure. First, we solve the equations and perform QR decompositions during a sufficiently long time, saving obtained matrices R_n to a file. Then, on the second pass, we generate random matrix C_{n_1} (see the details above) and perform the backward iterations, reading R_n from the file from the end to the beginning. When a sufficiently large number of transient iterations are made, we start to compute angles between contracting and expanding subspaces of the column space of C_n until we arrive at the beginning of the file of R_n.

The algorithm of computation of the angles between subspaces, the so-called principal angles, can be found, e.g., in Refs. [13,28]. Consider a matrix C_n. First of all, its columns must be classified as vectors associated with contracting and expanding directions of the tangent space, according to signs of corresponding Lyapunov exponents. Thus we obtain a matrix S comprising of n_s covariant Lyapunov vectors from the contracting subspace and a matrix U that consists of n_u vectors of the expanding subspace. It is natural to assume that $n_s > n_u$. For both of these matrices, we compute the QR factorizations $S = Q_s R_s$, $U = Q_u R_u$, and then compose the matrix M,

$$M = Q_s^T Q_u. \tag{A3}$$

Cosines of the sought principal angles θ_i, $(i = 1, \ldots, n_u)$ are equal to the singular values of the M, which can be easily computed (see, e.g., [13,29]).

This algorithm is known to fail to accurately compute very small angles and in Ref. [28], an improved version is suggested. But, nevertheless, we use the standard algorithm because the extremely high accuracy is not needed for our purposes.

[1] A. Katok and B. Hasselblatt, *Introduction to the Modern Theory of Dynamical Systems* (Cambridge University Press, New York, 1995).

[2] J. Guckenheimer and P. Holmes, *Nonlinear Oscillations, Dynamical Systems, and Bifurcations of Vector Fields* (Springer, New York, 2002).

[3] S. P. Kuznetsov, Phys. Rev. Lett. **95**, 144101 (2005).

[4] S. P. Kuznetsov and E. P. Seleznev, JETP **102**, 355 (2006).

[5] S. P. Kuznetsov and I. R. Sataev, Phys. Lett. A **365**, 97 (2007).

[6] P. V. Kuptsov, S. P. Kuznetsov, and I. R. Sataev, e-print arXiv:0804.3677.

[7] O. B. Isaeva, A. Y. Jalnine, and S. P. Kuznetsov, Phys. Rev. E **74**, 046207 (2006).

[8] S. P. Kuznetsov and A. Pikovsky, Physica D **232**, 87 (2007).

[9] S. P. Kuznetsov and A. Pikovsky, Europhys. Lett. **84**, 10013 (2008).

[10] S. P. Kuznetsov and V. I. Ponomarenko, Tech. Phys. Lett. **34**, 771 (2008).

[11] L. Young, Nonlinearity **21**, T245 (2008).

[12] F. Ginelli, P. Poggi, A. Turchi, H. Chaté, R. Livi, and A. Politi, Phys. Rev. Lett. **99**, 130601 (2007).

[13] G. H. Golub and C. F. van Loan, *Matrix Computations*, 3rd ed. (The Johns Hopkins University Press, Baltimore, MD, 1996).

[14] H. G. Schuster, *Deterministic Chaos: An Introduction* (Physik Verlag, Weinheim, 1984).

[15] E. Ott, *Chaos in Dynamics Systems* (Cambridge University Press, New York, 1993).

[16] N. N. Kalitkin, *Chislennye Metody (Numerical Methods, In Russian)* (Nauka, Moscow, 1978).

[17] W. F. Ames, *Numerical Methods for Partial Differential Equations* (Academic Press, New York, 1977).

[18] T. S. Parker and L. O. Chua, *Practical Numerical Algorithms*

for Chaotic Systems (Springer-Verlag, Berlin, 1989).
[19] S. Wolfram, *Theory and Applications of Cellular Automata, Advanced Series on Complex Systems* (World Scientific Publication, Singapore, 1986).
[20] K. Kaneko, Prog. Theor. Phys. **99**, 263 (1989).
[21] P. Manneville, *Macroscopic Modelling of Turbulent Flows*, Lecture Notes in Physics Vol. 230 (Springer-Verlag, Berlin, 1985), pp. 319–326.
[22] L. Keefe, Phys. Lett. A **140**, 317 (1989).
[23] L. Junge and U. Parlitz, Phys. Rev. E **61**, 3736 (2000).
[24] H. L. Yang, K. A. Takeuchi, F. Ginelli, H. Chaté, and G. Radons, Phys. Rev. Lett. **102**, 074102 (2009).
[25] J.-P. Eckmann and D. Ruelle, Rev. Mod. Phys. **57**, 617 (1985).
[26] K. Geist, U. Parlitz, and W. Lauterborn, Prog. Theor. Phys. **83**, 875 (1990).
[27] C. Skokos, e-print arXiv:0811.0882, Lect. Notes Phys. (to be published).
[28] A. V. Knyazev and M. E. Argentati, SIAM J. Sci. Comput. (USA) **23**, 2008 (2002).
[29] W. H. Press, S. A. Teukolsky, W. T. Vettering, and B. P. Flannery, *Numerical Recipes in C* (Cambridge University Press, New York, 1992).